Published in final edited form as:
Biochemistry. 2012 December 21; 51(51): 10208–10217. doi:10.1021/bi301243v.

Structure of Aminodeoxychorismate Synthase from *Stenotrophomonas maltophilia*†

Asim K. Bera[‖], **Vesna Atanasova**[‖], **Anjali Dhanda**[‖], **Jane E. Ladner**[‖,⊥], and **James F. Parsons**[*,‖]

Institute for Bioscience and Biotechnology Research, University of Maryland and National Institute of Standards and Technology, 9600 Gudelsky Drive, Rockville, Maryland 20850.

‖ University of Maryland ⊥ National Institute of Standards and Technology

Abstract

PabB, aminodeoxychorismate synthase, is the chorismic acid binding component of the heterodimeric PabAB complex that converts chorismic acid to 4-amino-4-deoxychorismate, a precursor of *p*-aminobenzoate and folic acid in microorganisms. The second component, a glutamine amidotransferase subunit, PabA, generates ammonia that is channeled to the PabB active site where it attacks the C4 carbon of a chorismate derived intermediate that is covalently bound, through C2, to an active site lysine residue. The presence of a PI**K**GT motif was, until recently, believed to be discriminate PabB enzymes from the closely related enzyme anthranilate synthase, which typically contains a PI**A**GT active site motif and does not form a covalent enzyme-substrate intermediate with chorismate. A subclass of PabB enzymes that employ an alternative mechanism requiring two equivalents of ammonia from glutamine and that feature a noncovalently bound 2-amino-2-deoxyisochorismate intermediate was recently identified. Here we report the 2.25 Å crystal structure of PabB from the emerging pathogen *Stenotrophomonas maltophilia.* It is the first reported structure of a PabB that features the PI**A**GT motif. Surprisingly, no dedicated *pabA* is evident in the genome of *S. maltophilia* suggesting that another cellular amidotransferase is able to fulfill the role of PabA in this organism. Evaluation of the ammonia-dependent aminodeoxychorismate synthase activity of *S. maltophilia* PabB alone revealed that it is virtually inactive. However, in the presence of a heterologous PabA surrogate, typical levels of activity were observed using either glutamine or ammonia as the nitrogen source. Additionally, the structure suggests that a key segment of the polypeptide can remodel itself to interact with a nonspecialized or shared amidotransferase partner *in vivo*. The structure and mass spectral analysis further suggest that *S. maltophilia* PabB, like *Escherichia coli* PabB, binds tryptophan in a vestigial regulatory site. The observation that the binding site is unoccupied in the crystal structure, however, suggests the affinity may be low relative to *E. coli* PabB.

†This work was supported in part by NIH Grant AI067530 (J.F.P.). Some data for this study were measured at beamline X29 at the National Synchrotron Light Source. Financial support comes principally from the Offices of Biological and Environmental Research and of Basic Energy Sciences of the US Department of Energy, and from the National Center for Research Resources of the National Institutes of Health.

* Address correspondence to this author. (J.F.P), parsonsj@umd.edu, phone 240-314-6158; Fax 240-314-6255..

Supporting Information Available. Purification protocols, One superposition illustration (Figure S1), LC/MS data including chromatograms (Figures S2, S4). ITC Data (Figure S3), Steady state kinetic data (Figures S5, S6). This material is available free of charge via the Internet at http://pubs.acs.org

Stenotrophomonas maltophilia is a complex, versatile, and ubiquitous aerobic Gram-negative bacterium (1). *S. maltophilia* is abundant in soil and endophytic strains have been isolated from many plants including key crops such as rice and wheat (2). While its association with plants is often beneficial and no phytopathogenic strains have been identified, *S. maltophilia* is a significant emerging human pathogen (1, 3). Typically a nosocomial concern, *S. maltophilia* infections are often associated with cystic fibrosis (CF)[1], severe immunosuppression, and cancer related hematologic disorders (4–7). Mortality rates attributable to *S. maltophilia* bacteremia range from 26 percent to over 60 percent (1, 8). The role of *S. maltophilia* in acute and long-term CF related lung disease remains somewhat controversial. It is clear that *S. maltophilia* is increasingly common in the CF lung flora; however, studies have reached disparate conclusions on the question of whether the organism negatively impacts lung function (5, 9, 10). Recent data, however, has shown that *S. maltophilia* may enhance the persistence of *Pseudomonas aeruginosa* infections *via* interspecies signaling and that *S. maltophilia* is likely a contributor in its own right to the long-term inflammatory damage to the lungs of CF patients (5, 11).

Much of the concern surrounding the emergence of *S. maltophilia* stems from its intrinsic antibiotic resistance. β-lactamase production, sophisticated multidrug efflux systems, biofilm formation, and other factors render many antibiotics ineffective against *S. maltophilia* (1, 12, 13). Trimethoprim-Sulfamethoxazole (TMP-SMX), an agent often disfavored due to toxicity and allergic concerns, is considered the primary therapeutic option for *S. maltophilia* infections (14, 15). The recent isolation of pandrug-resistant *S. maltophilia* exemplifies the severe threat posed by drug resistant Gram-negative bacteria (16).

TMP-SMX targets two enzymes in the folate pathway, dihydropteroate synthase and dihydrofolate reductase (17). The effectiveness of TMP-SMX illustrates that disabling folate production in *S. maltophilia* remains, in principle, a viable strategy. Our familiarity with the folate pathway and a curious mechanistic observation prompted us to investigate the details surrounding the synthesis of the folate precursor *p*-aminobenzoate in *S. maltophilia* (18, 19). The conversion of chorismic acid to *p*-aminobenzoate in bacteria typically involves three enzymes, PabA, -B, and -C. PabB catalyzes the amination of chorismate yielding 4-amino-4-deoxychorismate (ADC) and is a member of a family of structurally similar chorismate-utilizing enzymes that also includes anthranilate synthase (TrpE), isochorismate synthase, and salicylate synthase. PabA is an amidotransferase that supplies ammonia from glutamine hydrolysis and PabC is a pyridoxal phosphate-dependant enzyme that catalyzes the elimination of pyruvate from ADC, forming *p*-aminobenzoate (18). PabA and PabB must interact, at least transiently, for glutamine-dependant catalysis to occur (18). PabB, however, can use exogenous ammonia and does not strictly require PabA in order to produce ADC. Mechanistically, PabB enzymes are typically characterized by an active site lysine that attacks C2 of chorismate displacing the 4-OH group yielding a transient covalent intermediate (18, 20). The active site lysine is then displaced by nucleophilic attack of ammonia at C4 of the enzyme bound intermediate (Figure 1). Recently, however, Schadt et al. described a noncovalent mechanism involving a 2-amino-2-deoxyisochorismate (ADIC) intermediate that was unappreciated but is apparently characteristic of PabB from several organisms including *Bacillus subtilis*, the bioterror agent *B. anthracis*, and the emerging pathogen *S. maltophilia* (19). Instead of an active site lysine carrying out the initial attack on chorismate, in these enzymes, it is another ammonia molecule that attacks C2 of chorismate and displaces the 4-OH group. An alanine occupies the position analogous to that of catalytic lysine in the canonical PabB enzymes.

[1]Abbreviations: CF, cystic fibrosis; TMP-SMX, Trimethoprim-Sulfamethoxazole; ADC, 4-amino-4-deoxychorismate; ADIC, 2-amino-2-deoxyisochorismate; SmPabB, *Stenotrophomonas maltophilia* PabB; DHHA, *trans*-2,3-dihydro-3-hydroxyanthranilic acid.

In order to evaluate what structural differences accompany this alternative mechanism and to provide a starting point for structure based drug design efforts aimed at targeting an additional step in folate biosynthesis in *S. maltophilia*, we have conducted a structural, functional, and bioinformatic evaluation of *S. maltophilia* PabB (SmPabB). Here we report the 2.25 Å crystal structure of SmPabB. An unexpected trimer of dimers featuring a reorganized PabA interface region forms the basis of an unusually high solvent content crystal lattice. We confirm, using LC/MS that, like the *B. subtilis* PabB, SmPabB produces ADC via a noncovalent ADIC intermediate. Evaluation of the activity of the enzyme in light of the absence of a dedicated *pabA* reveals that SmPabB is virtually inactive alone but forms a high affinity complex with *E. coli* PabA suggesting the observed plasticity in the PabA interface region of SmPabB may promote *in vivo* accommodation of alternative or nonspecialized amidotransferase partners.

Experimental Procedures

Protein Expression and Purification

A synthetic construct containing *S. maltophilia pabB*, optimized for overexpression in *E. coli*, was obtained commercially (Genscript) and subcloned into the expression vector pET28a (Novagen). SmPabB was overexpressed in *E. coli* strain BL21(DE3) using the autoinduction method of Studier (21). Cells were grown initially at 37°C until the culture density reached an optical density of ~0.3 at 600 nm at which time the temperature of the shaking incubator was reduced to 20°C. The bacterial cells were then harvested by centrifugation after 14-16 h and stored at - 20° C until needed. SmPabB was purified by cobalt ion affinity chromatography essentially as directed by the resin manufacturer (Pierce). Human α-thrombin (Haematologic Technologies) was used to remove the portion of the fusion tag encoded by the pET-28a vector. Thrombin was then removed by passing the mixture over benzamidine agarose. The cleaved fusion tag was removed by a second passage over the cobalt resin. SmPabB judged pure by SDS-PAGE analysis was concentrated to ~13 mg/mL, dialyzed against 25 mM Tris, 1 mM DTT, 1 mM EDTA (pH 7.8) and stored in 0.2 mL aliquots at -80°C. SmPabB shows no particular tendency to aggregate and no noticeable loss of activity or precipitation were observed upon thawing after storage at -80 °C. Expression and purification procedures for *E. coli* PabA and PabC are described in the supporting information. *E. coli* PabB was purified as previously described (18).

Mass Spectral Identification of Intermediates and Products in SmPabB Catalyzed Reactions

LC/MS was used to confirm that SmPabB exhibited the predicted activity previously described for the *B. subtilis* PabB (19). ADIC, ADC, and *p*-aminobenzoate were positively identified using authentic standards of each compound (22). Reactions containing SmPabB and chorismate were subjected to liquid chromatography using a Waters Acquity UPLC system and a Waters HSS T3 2.1 × 100 mm UPLC column. The binary solvent system used for separation consisted of 0.1% formic acid (solvent *A*) and 0.1% formic acid in acetonitrile (solvent *B*). The chromatographic method time was five minutes and the following gradient profile was used: 0-1.5min, 5% *B*; 1.5-4.5min, a concave gradient (Waters type 7) to 95% *B*; 4.5-5.0 min, 95% *B*. The flow rate was 0.4 mL/min. Under these conditions the elution times were: ADC, 1.02 min; ADIC, 1.8 min, *p*-aminobenzoate, 3.8 min. MS identification was by means of an attached Waters LCT Premiere ESI-TOF mass spectrometer operating in positive ion mode.

Measurement of Enzymatic Activity

The ADC synthase activity of SmPabB was followed using a discontinuous HPLC based assay based on detection of *p*-aminobenzoate in reactions also containing recombinant PabC (ADC lyase) and in some cases, PabA, both from *E. coli.* ADC produced by PabB or PabA-PabB mixtures was converted to *p*-aminobenzoate and pyruvate by excess PabC. Reactions were performed at 25 °C in 20 mM HEPES, 5 mM $MgCl_2$, 0.1 mM DTT, 0.1 M glutamine, (pH 8.0). When exogenous ammonia was used as the ammonia source, glutamine was omitted from the buffer and 0.1M $NH_4(SO4)_2$ was included. Additional details for specific assays are given either in the corresponding figure or table legend, or in the supporting information.

Determination of the PabA7B Dissociation Constants by Fluorescence Titration

Steady-state fluorescence emission spectra from 300-400 nm (λ_{ex} = 290 nm) were obtained at 25 °C in 50 mM Hepes, 5 mM $MgCl_2$ (pH 8.0) using a Varian Eclipse fluorescence spectrometer. The K_d for the PabA-SmPabB complex was determined from the observed increase in tryptophan fluorescence as a function of increasing PabA concentration. The change in fluorescence at 340 nm was plotted as a function of PabA concentration and the data were fit to a quadratic plus linear function (Equation 1) where A represents the titration amplitude, S represents the offset from zero, [L] the PabA concentration, *n* the stoichiometry, and [P] the monomer concentration of SmPabB.

$$\Delta F = S + \frac{A^* \sqrt{(K_d[P]+n+[L])^2 - 4n[P][L]}}{2n[P]} + S\,[L] \quad (1)$$

Molecular Weight from Laser Light Scattering

The solution molecular mass of SmPabB was determined by a combination of laser light scattering and interferometric refractometry. 20 μL samples were injected onto a Shodex KW-802.5 gel filtration column attached to an Agilent 1100 series HPLC. Light scattering and concentration measurements were made using a DAWN EOS 18-angle light scattering detector (Wyatt Technology) and an OPTILAB DSP interferometric refractometer (Wyatt Technology). The column was equilibrated in 20 mM KH_2PO_4, 100 mM KCl, 0.2 mM EDTA, and 0.02% sodium azide (pH 6.5). A refractive index increment of 0.185 mL/g was used to estimate concentrations for molecular weight estimates, and bovine serum albumin was used as an isotropic scatterer for detector normalization to compensate for slight differences in the electronic gain of the 18 detectors. Molecular mass calculations were performed using ASTRA software (Wyatt Technology).

Crystallization

Initial crystallization screens of PabB were performed at ambient temperature using the sitting drop vapor diffusion method with commercially available screening kits. The protein solution was typically ~13 mg/mL prior to screening. Equal volumes of protein solution and reservoir solution, typically 2-4 μL total volume, were mixed for each experiment. Initial screening hits were optimized until, ultimately, a mixture containing 0.05 M $MgCl_2 \cdot 8H_2O$, 0.1 M HEPES, 12-15% w/v polyethylene glycol monomethylether 550, 0.1% CHAPS (pH 7.8) yielded the best results. Bipyramidal shaped (~0.1× 0.2× 0.4 mm) crystals were typically obtained after ~2 days and were cryopreserved in liquid nitrogen after a brief exposure to artificial mother liquor containing 30% polyethylene glycol monomethylether 550.

Collection and Processing of Crystallographic Data

Diffraction data for SmPabB was collected at National Synchrotron Light Source, Brookhaven National Laboratory on beamline X29 using a wavelength of 1.0809 Å. Crystals belonged to the $P6_322$ space group with one monomer per asymmetric unit and they diffracted to 2.25 Å. Diffraction data were scaled and processed using HKL2000 (23). Data collection statistics are presented in Table 1.

Structural Solution and Refinement

The structure of SmPabB was solved by molecular replacement using the program Phaser (24). The search model was PabB *E. coli* (PDB code 1K0G). The initial model was rebuilt using PHENIX auto builder to match the SmPabB sequence (25). The refinement procedure included periodic examinations of residues and subsequent refitting using the graphics program COOT (26). The model was completed and refined by using COOT for expanding the model and REFMAC5 for refining between building sessions (27). Solvent molecules were identified and included as the refinement progressed. The final model includes one magnesium ions, two CHAPS detergent molecules, and four PEG fragments, one of which is in the exposed active site. No density was observed for residues 286-297 or for residues 453-454 at the C-terminus. Refinement parameters and statistics are summarized in Table 1. The refined coordinates have been deposited in the Protein Data Bank as entry 4GRH.

Assay for Tryptophan Binding

LC/MS was used to assess whether purified SmPabB preparations contained noncovalently bound tryptophan. A 50 μL sample of SmPabB identical to those used for crystallization experiments was thawed and diluted tenfold with an aqueous mixture of 50% acetonitrile and 1% formic acid. After passage through a 10 kilodalton cutoff filter by centrifugation, 2 μL aliquots were analyzed by LC/MS. Similar analyses were conducted using *E. coli* PabB, *E. coli* MenF, and the ADIC synthase PhzE from *Pseudomonas aeruginosa*, all of which were previously purified in our lab (18, 28). Purification of PhzE described in supporting information.

Isothermal Titration Calorimetry

The interaction between SmPabB and tryptophan was analyzed using a Microcal iTC200 calorimeter. The titrant syringe contained 1 μM tryptophan and the cell contained 100 μM SmPabB. The cell was maintained at 25°C. An initial 0.5 μL injection and 34 1 μL injections were made. The spacing between injections was 180 s. Data were analyzed using Origin 7 software as described in the legend to figure S3.

Results and Discussion

Bioinformatic Analysis of p7Aminobenzoate Biosynthesis in S. maltophilia

While a few bacteria can acquire folates from their environment, most bacteria must make their own folates in order to survive and grow (29). The effectiveness of TMP-SMX against *S. maltophilia* illustrates that folate production is a required function in this organism. *S. maltophilia* K279a, a clinical isolate, has been sequenced and much of the folate biosynthetic machinery, including *pabB* (Smlt1032), is readily identifiable (12). Confusion, however, surrounds the identity of PabA and PabC (ADC lyase) in *S. maltophilia*. There is apparently no dedicated *pabA* gene in the *S. maltophilia* K279a genome raising the question of how the organism makes ADC and *p*-aminobenzoate for folate production. Furthermore, the gene adjacent to *pabB* is erroneously annotated as *pabC* (Smlt1034) in *S. maltophila.* The misidentification of Smlt1034 homologs as ADC lyase has, in fact, become entrenched throughout bioinformatic databases. The PDB, for example, features the structure of an

Smlt1034 homolog from *E. coli* (2R1F; 46% identical to Smlt1034) that was deposited as "predicted ADC lyase from *E. coli*" despite there being no evidence to support the annotation and despite the fact that the structure of the true PabC from *E. coli* has been in the PDB for nearly a decade (1I2K and others) and bears no resemblance to 2R1F. While the identity of the *S. maltophilia* PabC remains uncertain, we have identified Smlt1373 as a candidate. It is 27% identical (E = 0.005) to the legitimate PabC from *P. aeruginosa* (PDB code: 2Y4R) but not detectably similar (using the same BLAST algorithm parameters) to the *E. coli* PabC (1I2K). Despite the incongruous BLAST results, many of the key PabC active site residues can be identified in Smlt1373 including K140, the residue that forms the Schiff base linkage with the required PLP cofactor.

In terms of the identity of PabA, one possibility is that *S. maltophilia* uses TrpG (Smlt4311), its anthranilate synthase glutamine amidotransferase subunit, in a second role as the ammonia donor for *p*-aminobenzoate biosynthesis. A similar dual function amidotransferase has been described previously in *Bacillus* (30). Interestingly, the putative dual function amidotransferase in *B. subtilis* (BSU00750) is encoded adjacent to *pabB* rather than being located in the *trp* operon. Alternative and less likely possibilities are that SmPabB functions with an unrecognizable PabA partner or has a novel ability to generate ammonia from glutamine without aid of another polypeptide. There are example of fused ADC synthases, both PabAB and PabBC fusions are known, however, at just 49 kDa SmPabB does not appear to be among these.

In order to conduct a timely analysis of SmPabB to complement the reporting of the structure, we elected to use PabA and PabC from *E. coli* in assays of ADC and *p*-aminobenzoate production by SmPabB.

Overall Structure of SmPabB and Crystal Packing

SmPabB is a 454 amino acid, ~49.5 kDa protein that exhibits the complex α/β fold characteristic of the family of chorismate utilizing enzymes that, in addition to PabB (Figure 2A), includes anthranilate synthase (TrpE), salicylate synthase, and isochorismate synthase (18, 28, 31). The monomer is best described as a sandwich of two β-sheets with α-helices on the outside (Figures 2A, 4). Crystals of SmPabB grown during this study had an unusually high solvent content of 71.7% and a corresponding Matthews coefficient of 4.36 $Å^3$/Da. Figures 2B-D illustrate the arrangement of SmPabB monomers in the crystal lattice. Each unit cell contains 12 monomers arranged as two trimers of dimers. These hexameric units interact in a manner that yields a large pore or solvent channel in the crystal lattice (Figure 2B) that contributes to the unusually high solvent content of the crystal. The arrangement of subunits that the lattice is built upon is shown in figure 2D and features a continuous β-sheet between two SmPabB monomers. The segment of SmPabB involved in this interaction (residues 286-297) corresponds to a key, normally α-helical segment, that is often disordered in the absence of substrate and/or the glutaminase subunit, PabA (18). Figures 3 and S1 illustrate the dramatically different orientations of this flexible segment that is found in all PabB-like chorismate utilizing enzymes. In the TrpE-G complex, the segment is a well defined helix that forms part of the interface with the TrpG glutaminase subunit and contributes key elements of the active site notably two of the four acidic residues that coordinate the active site magnesium ion (28, 31). The corresponding segment of SmPabB, in the structure presented here, appears to have been recruited and remodeled as a key element of the continuous β-sheet between two SmPabB monomers that forms during the crystallization process (Figure 2D). This behavior may be emblematic of an adaptable interface region that even when unstructured, does not cause irreversible aggregation or destabilization of the overall polypeptide. In addition, it may suggest an ability to cope with nonspecialized amidotransferase partners in the apparent absence of a dedicated PabA subunit. Despite the unusual crystal packing observed, however, laser light scattering

experiments conducted on SmPabB confirmed that it, like *E. coli* PabB, is a monomer in solution with an apparent mass of 48.6 ± 0.9 kDa.

Ligand Binding Sites

PabB-type chorismate utilizing enzymes all have an active site that binds chorismate and some enzymes, notably TrpE and at least one PabB, have an additional binding site that accommodates tryptophan. In the case of TrpE, tryptophan binding is part of a feedback regulatory mechanism that limits the overproduction of tryptophan. In PabB, which is thought to have evolved from TrpE (18), it is believed the site is a nonfunctional vestigial binding site. The locations of the two potential ligand binding sites present in each monomer of SmPabB are illustrated in Figure 4. The chorismate binding site is composed of amino acid residues contributed both by the β-sheet core and by two key α-helices, one of which is the segment remodeled as a β-strand (residues 300-309) and the other is the long C-terminal helix (residues 432-452). A more detailed description of the active site is provided below.

The putative vestigial tryptophan binding site, first identified in *E. coli* PabB, appears to be present in SmPabB as well, though it is unoccupied in the structure described here. We previously reported that tryptophan bound to the vestigial site in *E. coli* PabB either had evolved to serve a structural role or was simply bound so tightly that it could not be readily removed (18). In anthranilate synthase, tryptophan binding to an analogous site regulates the activity of the enzyme by stabilizing an active site conformation that is not conducive to catalysis (31). In all cases, the tryptophan binding site is located some 15 Å from the active site and it is composed exclusively of residues from the β-sheet sandwich and the associated loops between the β-strands (Figure 4).

Similarity to Known PabB Structures

SmPabB is just the third ADC synthase (PabB) structure to be solved and the first that uses the noncovalent intermediate mechanism described by Schadt et al. (19). The results of conducting automated structural alignments of SmPabB with the known PabB structures and with other relevant structural homologs are shown in Table 2 (32). The final model of SmPabB consists of 439 of the 454 residues in the native sequence. The larger of the two disordered internal regions that could not be modeled, residues 286-297, is a helical segment that is also partially or entirely disordered in the two other known PabB structures, from *E. coli* (1K0E, 1K0G; two crystal forms (18)) and from the cellulose degrading Gram-negative bacteria *Cytophaga hutchinsonii* (3H9M). Based on analysis of and comparison to heterodimeric anthranilate synthase (TrpEG) structures (31, 33), this helix is predicted to be part of the PabAB interface and likely becomes ordered upon PabAB complex formation. The shorter disordered segment (residues 37-39) is located near the putative tryptophan binding site and on a solvent exposed loop. Finally, no density was observed for the two C-terminal residues of SmPabB.

While some disorder is present in the structures of both *E. coli* PabB and SmPabB, it is clear that all major structural elements are conserved between these two proteins. The *C. hutchinsonii* PabB was a structural genomics deposition to the PDB has not been described by any publication. Interestingly, two elements of that structure differ from the SmPabB and *E. coli* PabB structures. The *C. hutchinsonii* PabB lacks two β-strands that form one end of one of the long β-sheets of each monomer. In SmPabB this corresponds to residues 60-70 and *E. coli* PabB, residues 63-78. While the significance of this is unclear, we had previously noted that these strands are also absent in the archeabacterial *Sulfolobus* TrpE structure (1QDL) but are present in the known eubacterial TrpE structures ((34)1I1Q, 1I1S). Additionally, SmPabB and *E. coli* PabB both feature a long loop region (Figure 4; residues ~90-105) that forms a partial flap over the vestigial tryptophan binding site identified in *E.*

coli PabB. The corresponding loop in *C. hutchinsonii* PabB is only four residues (77-81). Tryptophan was not included in the *C. hutchinsonii* PabB model but it is unknown whether the shorter loop plays a major role in tryptophan binding and the data presented here and elsewhere suggest other factors are also important (18, 35). The missing strands and the shortened loop together account for the shorter length of *C. hutchinsonii* PabB (426 residues) when compared to SmPabB (454 residues) and *E. coli* PabB (453 residues).

Active Site

The SmPabB chorismate binding site is highly distorted and disordered. Ligand-bound structures of anthranilate synthase and isochorismate synthase have revealed that a ligand-Mg^{2+} complex is formed that ties together several secondary structural elements and promotes a closed active site conformation (31, 36). Four acidic residues in particular, on two parallel helical segments, tie the active site together by interacting with the active site Mg^{2+} ion. In *E. coli* PabB, three Glu residues (302, 436, and 439) and Asp299 coordinate the Mg^{2+} ion either directly or via water molecules. In SmPabB the four corresponding residues are all Glu residues (298, 301, 435, and 438). Two of these residues, however, Glu298 and Glu301 are located on the remodeled helix-turned-sheet element that forms the intersubunit β-sheet in the SmPab structure (Figures 2D, 3). This arrangement places these residues some 15 Å from their expected location in a closed enzyme-substrate complex. In addition to close analogs or actual products, the known structures of *E. coli* PabB and isochorismate synthase illustrate that even seemingly poor substrates mimics such as formate and phosphate ions can promote a closed or partially closed conformation (18, 28). Kinetic data presented below suggest, however, that the interaction of SmPabB with an amidotransferase partner also has a significant, perhaps greater effect on active site organization. Based on an evaluation of TrpEG complexes, the disordered regions of SmPabB are likely part of the PabAB interface in addition to contributing two of the four Glu residues involved in Mg^{2+} coordination (Figures 3, 4).

One magnesium ion was identified in the SmPabB structure but it is located outside of the active site and its location suggests it has no physiologic relevance. The octahedral coordination involves five water molecules and the carboxylate groups of Glu284 and Glu331. The latter interacts indirectly via a water molecule while Glu284 interacts directly with the magnesium ion.

The ^{273}PI**A**GT^{277} motif that differentiates SmPabB mechanistically from *E. coli* PabB and other canonical PabB enzymes is engaged in several interactions that hold it in a distorted conformation in the absence of substrate (Figure 5). Ile274, in particular, is engaged in two interactions that hold the motif in its observed location. The backbone amide of Ile274 is 2.5 Å from the side chain carboxyl of Glu258 and the side chain of Ile274 is sandwiched between the phenyl ring of Phe241 and the nonpolar portion of the Agr259. These interactions are likely of no functional significance but rather reflect favorable contacts that form in the absence of substrate and/or PabA. Following Thr277, the chain meanders in an unstructured fashion until the chain becomes disordered to the extent that no density was visible for residues 286-297.

Tryptophan Binding and the Vestigial Trp Binding Site of SmPabB

Upon solving the structure of *E. coli* PabB, we surprisingly observed tryptophan bound to a vestigial site analogous to the regulatory binding site in TrpE, a tryptophan biosynthetic enzyme (18). Since *E. coli* PabB remained the only known PabB structure for some time, it was difficult to assess whether tryptophan binding is common among PabB enzymes or what its importance might be. The structures of SmPabB and *C. hutchinsonii* PabB have now afforded an opportunity to further examine whether tryptophan binding is typical among

PabB enzymes. Tryptophan was ultimately not found in the SmPabB structure, however, a comparison with the *E. coli* PabB structure revealed significant similarity in putative binding site. Interestingly, examination of the analogous site in *C. hutchinsonii* PabB revealed that the side chain of Phe46 is wedged into the analogous site of that protein, likely preventing tryptophan from binding. A similar observation was made in the structure of the ADIC synthase PhzE where Trp184 occupies the site and likely blocks exogenous tryptophan binding (37). While SmPabB does have a tryptophan residue (Trp43) that corresponds to Trp184 of PhzE and Phe46 of *C. hutchinsonii* PabB its orientation is more consistent with Phe46 of *E. coli* PabB, which does not block tryptophan binding. Thus, while tryptophan was not observed bound to SmPabB nothing appeared to rule out the possibility that it could bind.

Three experiments were pursued to evaluate whether SmPabB binds tryptophan despite its absence in the crystal structure. First, we used LC/MS to examine whether purified solutions of SmPabB contained tryptophan. Figure S2 illustrates that tryptophan is clearly present in samples of SmPabB identical to those used for crystallization experiments. We conducted a similar analysis on three SmPabB homologs: *E. coli* PabB, *E. coli* MenF (isochorismate synthase), and *Pseudomonas aeruginosa* PhzE (ADIC synthase). The latter two were not believed to bind tryptophan based on crystallographic data (18, 28, 35, 37). The results show that *E. coli* PabB samples, as expected, contained tryptophan while the MenF and PhzE samples did not (Figure S2). Second, we used isothermal titration calorimetry to show that SmPabB and tryptophan form a complex characterized by a dissociation constant of ~11.7 μM (Figure S3). Deviation from the expected 1:1stoichiometry and further analysis by LC/MS confirmed that extensive dialysis did not remove all tryptophan prior to the calorimetric analysis. Finally, co-crystallization and soaking experiments were conducted in order to determine whether higher tryptophan concentrations could yield a tryptophan-bound SmPabB structure. Soaking experiments have thus far yielded promising but inconclusive results as data sets appear to show obvious density consistent with tryptophan bound in the expected location, however, no data set extends beyond ~3 Å and they suffer other issues that prevent them from refining satisfactorily.

Interestingly, it appears SmPabB and TrpE have roughly the same affinity for tryptophan (38). As with *E. coli* PabB, however, addition of tryptophan had no effect on the activity of SmPabB.

Enzymatic Activity of SmPabB

Reactions containing SmPabB, *E. coli* PabA, chorismate, and glutamine were analyzed by LC/MS to determine whether SmPabB, like *B. subtilis* PabB, catalyzed the formation of ADC via an ADIC intermediate. Figure 6 illustrates that both ADIC and ADC were formed as predicted. Qualitative evaluation of the chromatographic data suggested that the conversion of ADIC to ADC was potentially rate limiting since ADIC appears to accumulate. However, further investigation showed that ADIC is released into solution prior to being rebound and converted to ADC in a second SmPabB-catalyzed reaction. Competition from the initially high amount of chorismate present also favors accumulation of ADIC that becomes unbound. In order to confirm that ADIC was free in solution, we included, in some assays, catalytic amounts of the enzyme PhzD from *P. aeruginosa*, which acts very efficiently on ADIC, in SmPabB containing reactions (22). This resulted in accumulation of the PhzD product 2,3-dihydro-3-hydroxyanthranilate (DHHA) and confirmed that SmPabB does not effectively sequester the ADIC intermediate (Figure S4).

Kinetic Characterization of SmPabB

Analysis of the kinetics of the glutamine and PabA-dependent conversion of chorismate to ADC revealed that SmPabB behaved much like the *B. subtilis* PabB (Figures S5, S6; (19)). SmPabB has a somewhat lower K_m for chorismate, 240 μM vs 410 μM for the *B. subtilis* enzyme, but both of these enzymes have K_m values for chorismate that are markedly higher than what has been described for the *E. coli PabB* (~13 μM (20)).

Analysis of ADC formation using purified ADIC to examine only the second half of the reaction, revealed that the second step is actually somewhat faster (k_{cat} ~ 0.02 s^{-1}) than the overall reaction (k_{cat} ~ 0.007 s^{-1}) and that initial accumulations of ADIC (Figure 6) are likely a consequence of the second step being slow at very low initial ADIC concentrations and high initial chorismate concentrations.

Effect of PabA on the Activity of SmPabB

Assays containing only SmPabB, chorismate ammonia, and PabC indicated that SmPabB was a very poor catalyst. When assays were conducted with 500 μM chorismate, the specific activity was 2×10^{-4} s^{-1}. Addition of equimolar *E. coli* PabA, however, significantly enhanced the reaction rate, even in the absence of glutamine as the ammonia donor. When assayed again at 500 μM chorismate, the specific activity increased 20-fold to 0.004 s^{-1} in the presence of PabA.

We first attempted to characterize the association of SmPabB and PabA by examining the dependence of the reaction rate on the ratio of PabA:SmPabB. The results suggested that the association was likely very strong. However, we were unable to drop the enzyme concentrations in these assays far enough to reliably estimate the binding constant due the sensitivity level of the assay system. Therefore we examined the PabA:SmPabB interaction directly by fluorescence titration. The results are shown in Figure 7 and reveal that *E. coli* PabA and SmPabB form a surprisingly tight complex characterized by a ~40 nM dissociation constant. This result supports the possibility that SmPabB has an adaptable interface region that may accommodate a variety of nonspecialized amidotransferase partners. A similar analysis of the interaction of *E. coli* PabA and PabB revealed a dissociation constant of 109 ± 58 nM.

Crystallographic evidence currently available for chorismate utilizing enzymes suggests that an occupied active can lead to structures that better reflect an active conformation. The structure of the enterobactin specific isochorismate synthase (EntC), for example, in complex with the product isochorismate features a well ordered, closed active site (36). Similarly, anthranilate synthase structures are well ordered in the presence of ligands (31). No structures of PabB have yet been solved with substrates or products present in the active site, however a simple formate ion found in the *E. coli* PabB active site does significantly reduce disorder relative to the completely unliganded structure (18). The formate is likely a mimic of the pyruvyl portion of chorismate as it binds in the same location and orientation as pyruvate in anthranilate synthase and the pyruvyl portion of isochorismate in the EntC structure. It is worth noting that the formate bound structure of *E. coli* PabB was obtained from crystals grown from solutions containing 2 M sodium formate a condition which may have favored occupancy of even a poor substrate mimic.

One explanation for the difficulty in obtaining substrate or product bound PabB structures is that chorismate may simply have little affinity for PabB in the absence of a PabA partner. This seems plausible in light of the disordered elements observed in all PabB structures solved to date. It may be that substrate alone cannot effectively promote the formation of an ordered PabB active site. In the case of SmPabB, evidence suggests that PabA:SmPabB

complex formation reduces SmPabB disorder based on the enhanced catalytic performance of the enzyme in the presence of PabA.

Comparison of E. coli PabA and S. maltophilia TrpG

In order to better understand why *E. coli* PabA was able to effectively partner with SmPabB, we compared the residues from each that are expected to form the PabB interface. Using PDBSum (39) we identified 26 residues from *S. marcescens* TrpG that contact the TrpE subunit in the anthranilate synthase complex structure 1I7Q (31). We then identified the corresponding residues in *E. coli* PabA and *S. maltophilia* TrpG by examining sequence alignments. Nearly 81 percent (21/26) of these residues are identical between *E. coli* PabA and *S. maltophilia* TrpG. Two others are conservative substitutions and just three likely interface residues are not conserved. Cys20, Glu21, and Lys29 of *E. coli* PabA correspond to *S. maltophilia* TrpG residues Gln20, Thr21, and Val29. These observations, along with the overall identity (61%) between the two proteins likely also contribute to the observed ability of *E. coli* PabA to serve SmPabB effectively. Additionally, the kinetic data showing that the SmPabB:*E. coli* PabA complex has activity equal to the *B. subtilis* PabAB (19) complex suggests that *E. coli* PabA may be maximizing the abilities of SmPabB. The much lower sequence identity (Table 2) between SmPabB, *E. coli* PabB, and TrpE coupled with the disorder observed in all PabB structures makes conducting a similar analysis of the PabA interface of PabB difficult.

Conclusion

The structure of SmPabB, the chorismate-binding subunit of the heterodimeric ADC synthase complex from the *S. maltophilia* folate pathway, has been solved. It is just the third reported PabB structure and it is the first described structure of a PabB that uses the alternative, and until recently unrecognized mechanism involving a noncovalent ADIC intermediate (19). The structure is notable for the very high solvent content of the crystals and the unusual trimer-of-dimers structure that the normally monomeric SmPabB adapts in the crystals form (Figure 2). Key elements of the typically disordered PabA interface region of SmPabB are reorganized to form a PabB:PabB interface that is a key part of the crystal lattice.

Surprisingly, *S. maltophila* does not appear to encode a dedicated PabA and may rely on the product of *trpG*, which is found adjacent to *trpE,* to serve as the amidotransferase partner for both enzymes. Evaluation of the activity of SmPabB revealed that the enzyme is a very poor catalyst in the presence of only chorismate and exogenous ammonia (from ammonium sulfate). Inclusion of a surrogate PabA (from *E. coli*), however, stimulated activity 20-fold even in the absence of glutamine suggesting that an amidotransferase partner can stabilize a more productive conformation of SmPabB even if it is not supplying ammonia to the reaction via glutamine hydrolysis. Fluorescence titration experiments indicate that SmPabB and *E. coli* PabA from a very stable complex. Together, the data are consistent with a scenario where SmPabB alone has minimal activity due to inherent disorder in key elements of the active site. Substrate binding alone is not enough to stabilize a productive conformation. Only when an amidotransferase partner is present would SmPabB produce ADC for conversion to *p*-aminobenzoate by PabC.

Evaluation of the regulatory controls on the transcription of both *pabB* and the *trp* operon components in *S. maltophilia* may reveal how the organism is able to regulate the production of both folate and tryptophan precursors using a single amidotransferase enzyme. The situation appears different than in *Bacillus* since the apparent bifunctional amidotransferase is not located in the folate operon in *S. maltophila* (as it is in *B. subtilis*), but rather adjacent to *trpE*. In order to obtain a SmPabB structure with a well organized active site, it seems

clear based on the three available PabB structures that a PabAB complex structure will ultimately be necessary.

Supplementary Material

Refer to Web version on PubMed Central for supplementary material.

References

1. Brooke JS. Stenotrophomonas maltophilia: an emerging global opportunistic pathogen. Clin. Microbiol. Rev. 2012; 25:2–41. [PubMed: 22232370]
2. Ryan RP, Monchy S, Cardinale M, Taghavi S, Crossman L, Avison MB, Berg G, van der Lelie D, Dow JM. The versatility and adaptation of bacteria from the genus Stenotrophomonas. Nat. Rev. Microbiol. 2009; 7:514–525. [PubMed: 19528958]
3. Abbott IJ, Slavin MA, Turnidge JD, Thursky KA, Worth LJ. Stenotrophomonas maltophilia: emerging disease patterns and challenges for treatment. Expert Rev Anti Infect Ther. 2011; 9:471–488. [PubMed: 21504403]
4. Di Bonaventura G, Pompilio A, Zappacosta R, Petrucci F, Fiscarelli E, Rossi C, Piccolomini R. Role of excessive inflammatory response to Stenotrophomonas maltophilia lung infection in DBA/2 mice and implications for cystic fibrosis. Infect. Immun. 2010; 78:2466–2476. [PubMed: 20308302]
5. Garazi M, Singer C, Tai J, Ginocchio CC. Bloodstream infections caused by Stenotrophomonas maltophilia: a seven-year review. J. Hosp. Infect. 2012; 81:114–118. [PubMed: 22494851]
6. Safdar A, Rolston KV. Stenotrophomonas maltophilia: changing spectrum of a serious bacterial pathogen in patients with cancer. Clin. Infect. Dis. 2007; 45:1602–1609. [PubMed: 18190323]
7. Denton M, Kerr KG. Microbiological and clinical aspects of infection associated with Stenotrophomonas maltophilia. Clin. Microbiol. Rev. 1998; 11:57–80. [PubMed: 9457429]
8. Senol E, DesJardin J, Stark PC, Barefoot L, Snydman DR. Attributable mortality of Stenotrophomonas maltophilia bacteremia. Clin. Infect. Dis. 2002; 34:1653–1656. [PubMed: 12032905]
9. Waters V, Atenafu EG, Salazar JG, Lu A, Yau Y, Matukas L, Tullis E, Ratjen F. Chronic Stenotrophomonas maltophilia infection and exacerbation outcomes in cystic fibrosis. J. Cyst. Fibros. 2012; 11:8–13. [PubMed: 21849265]
10. Waters VJ, Gómez MI, Soong G, Amin S, Ernst RK, Prince A. Immunostimulatory properties of the emerging pathogen Stenotrophomonas maltophilia. Infect. Immun. 2007; 75:1698–1703. [PubMed: 17220304]
11. Twomey KB, O'Connell OJ, McCarthy Y, Dow JM, O'Toole GA, Plant BJ, Ryan RP. Bacterial cis-2-unsaturated fatty acids found in the cystic fibrosis airway modulate virulence and persistence of Pseudomonas aeruginosa. ISME J. 2011
12. Crossman LC, Gould VC, Dow JM, Vernikos GS, Okazaki A, Sebaihia M, Saunders D, Arrowsmith C, Carver T, Peters N, Adlem E, Kerhornou A, Lord A, Murphy L, Seeger K, Squares R, Rutter S, Quail MA, Rajandream M-A, Harris D, Churcher C, Bentley SD, Parkhill J, Thomson NR, Avison MB. The complete genome, comparative and functional analysis of Stenotrophomonas maltophilia reveals an organism heavily shielded by drug resistance determinants. Genome Biol. 2008; 9:R74. [PubMed: 18419807]
13. Sanchez MB, Hernandez A, Martinez JL. Stenotrophomonas maltophilia drug resistance. Future Microbiol. 2009; 4:655–660. [PubMed: 19659422]
14. Falagas ME, Valkimadi P-E, Huang Y-T, Matthaiou DK, Hsueh P-R. Therapeutic options for Stenotrophomonas maltophilia infections beyond co-trimoxazole: a systematic review. J. Antimicrob. Chemother. 2008; 62:889–894. [PubMed: 18662945]
15. Farrell DJ, Sader HS, Jones RN. Antimicrobial susceptibilities of a worldwide collection of Stenotrophomonas maltophilia isolates tested against tigecycline and agents commonly used for S. maltophilia infections. Antimicrob. Agents Chemother. 2010; 54:2735–2737. [PubMed: 20368399]

16. Tan C-K, Liaw S-J, Yu C-J, Teng L-J, Hsueh P-R. Extensively drug-resistant Stenotrophomonas maltophilia in a tertiary care hospital in Taiwan: microbiologic characteristics, clinical features, and outcomes. Diagn. Microbiol. Infect. Dis. 2008; 60:205–210. [PubMed: 17950557]
17. Bushby SR. Synergy of trimethoprim-sulfamethoxazole. Can Med Assoc J. 1975; 112:63–66. [PubMed: 1093654]
18. Parsons JF, Jensen PY, Pachikara AS, Howard AJ, Eisenstein E, Ladner JE. Structure of Escherichia coli aminodeoxychorismate synthase: architectural conservation and diversity in chorismate-utilizing enzymes. Biochemistry. 2002; 41:2198–2208. [PubMed: 11841211]
19. Schadt HS, Schadt S, Oldach F, Süssmuth RD. 2-Amino-2-deoxyisochorismate is a key intermediate in Bacillus subtilis p-aminobenzoic acid biosynthesis. J. Am. Chem. Soc. 2009; 131:3481–3483. [PubMed: 19275258]
20. He Z, Stigers Lavoie KD, Bartlett PA, Toney MD. Conservation of mechanism in three chorismate-utilizing enzymes. J. Am. Chem. Soc. 2004; 126:2378–2385. [PubMed: 14982443]
21. Studier FW. Protein production by auto-induction in high density shaking cultures. Protein Expr. Purif. 2005; 41:207–234. [PubMed: 15915565]
22. Parsons JF, Calabrese K, Eisenstein E, Ladner JE. Structure and mechanism of Pseudomonas aeruginosa PhzD, an isochorismatase from the phenazine biosynthetic pathway. Biochemistry. 2003; 42:5684–5693. [PubMed: 12741825]
23. Otwinowski Z, Minor W. Processing of X-ray Diffraction Data Collected in Oscillation Mode. Methods in Enzymology. 1997; 276:307–326.
24. McCoy AJ, Grosse-Kunstleve RW, Adams PD, Winn MD, Storoni LC, Read RJ. Phaser crystallographic software. J Appl Crystallogr. 2007; 40:658–674. [PubMed: 19461840]
25. Zwart PH, Afonine PV, Grosse-Kunstleve RW, Hung L-W, Ioerger TR, McCoy AJ, McKee E, Moriarty NW, Read RJ, Sacchettini JC, Sauter NK, Storoni LC, Terwilliger TC, Adams PD. Automated structure solution with the PHENIX suite. Methods Mol. Biol. 2008; 426:419–435. [PubMed: 18542881]
26. Emsley P, Lohkamp B, Scott WG, Cowtan K. Features and development of Coot. Acta Crystallogr. D Biol. Crystallogr. 2010; 66:486–501. [PubMed: 20383002]
27. Murshudov GN, Skubák P, Lebedev AA, Pannu NS, Steiner RA, Nicholls RA, Winn MD, Long F, Vagin AA. REFMAC5 for the refinement of macromolecular crystal structures. Acta Crystallogr. D Biol. Crystallogr. 2011; 67:355–367. [PubMed: 21460454]
28. Parsons JF, Shi KM, Ladner JE. Structure of isochorismate synthase in complex with magnesium. Acta Crystallogr. D Biol. Crystallogr. 2008; 64:607–610. [PubMed: 18453696]
29. de Crécy-Lagard V, El Yacoubi B, de la Garza RD, Noiriel A, Hanson AD. Comparative genomics of bacterial and plant folate synthesis and salvage: predictions and validations. BMC Genomics. 2007; 8:245. [PubMed: 17645794]
30. Slock J, Stahly DP, Han CY, Six EW, Crawford IP. An apparent Bacillus subtilis folic acid biosynthetic operon containing pab, an amphibolic trpG gene, a third gene required for synthesis of para-aminobenzoic acid, and the dihydropteroate synthase gene. J. Bacteriol. 1990; 172:7211–7226. [PubMed: 2123867]
31. Spraggon G, Kim C, Nguyen-Huu X, Yee MC, Yanofsky C, Mills SE. The structures of anthranilate synthase of Serratia marcescens crystallized in the presence of (i) its substrates, chorismate and glutamine, and a product, glutamate, and (ii) its end-product inhibitor, L-tryptophan. Proc Natl Acad Sci U S A. 2001; 98:6021–6026. [PubMed: 11371633]
32. Holm L, Sander C. Dali: a network tool for protein structure comparison. Trends Biochem. Sci. 1995; 20:478–480. [PubMed: 8578593]
33. Knochel T, Ivens A, Hester G, Gonzalez A, Bauerle R, Wilmanns M, Kirschner K, Jansonius JN. The crystal structure of anthranilate synthase from Sulfolobus solfataricus: functional implications. Proc Natl Acad Sci U S A. 1999; 96:9479–9484. [PubMed: 10449718]
34. Parsons JF, Jensen PY, Pachikara AS, Howard AJ, Eisenstein E, Ladner JE. Structure of Escherichia coli aminodeoxychorismate synthase: architectural conservation and diversity in chorismate-utilizing enzymes. Biochemistry. 2002; 41:2198–2208. [PubMed: 11841211]

35. Kolappan S, Zwahlen J, Zhou R, Truglio JJ, Tonge PJ, Kisker C. Lysine 190 is the catalytic base in MenF, the menaquinone-specific isochorismate synthase from Escherichia coli: implications for an enzyme family. Biochemistry. 2007; 46:946–953. [PubMed: 17240978]
36. Sridharan S, Howard N, Kerbarh O, Błaszczyk M, Abell C, Blundell TL. Crystal structure of Escherichia coli enterobactin-specific isochorismate synthase (EntC) bound to its reaction product isochorismate: implications for the enzyme mechanism and differential activity of chorismate-utilizing enzymes. J. Mol. Biol. 2010; 397:290–300. [PubMed: 20079748]
37. Li Q-A, Mavrodi DV, Thomashow LS, Roessle M, Blankenfeldt W. Ligand binding induces an ammonia channel in 2-amino-2-desoxyisochorismate (ADIC) synthase PhzE. J. Biol. Chem. 2011; 286:18213–18221. [PubMed: 21454481]
38. Caligiuri MG, Bauerle R. Identification of amino acid residues involved in feedback regulation of the anthranilate synthase complex from Salmonella typhimurium. Evidence for an amino-terminal regulatory site. J Biol Chem. 1991; 266:8328–8335. [PubMed: 2022650]
39. Laskowski RA. PDBsum new things. Nucleic Acids Res. 2009; 37:D355–359. [PubMed: 18996896]

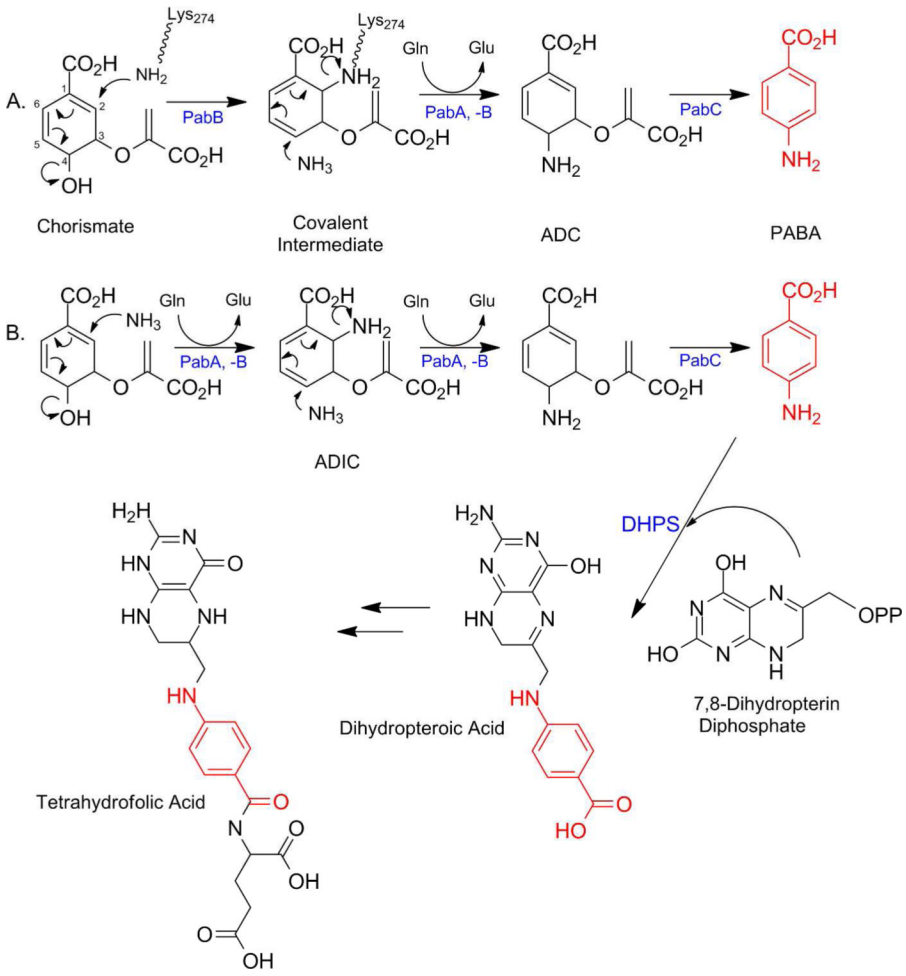

Figure 1.

Two schemes for the conversion of chorismate to ADC and the incorporation of *p*-aminobenzoate into folates. (A) PabB enzymes such as *E. coli* PabB that contain the ^{272}PI**K**GT^{276} motif catalyze the formation of a covalent C2-lysyl intermediate that is released by subsequent attack of ammonia at C4. (B) Less common PabB enzymes such as SmPabB that contain a PI**A**GT motif and require two equivalents of ammonia and produce a noncovalently bound ADIC intermediate. In both cases, PabC converts ADC to *p*-aminobenzoate in a PLP-dependent elimination reaction. *p*-aminobenzoate is then incorporated into the folate precursor dihydropteroic acid.

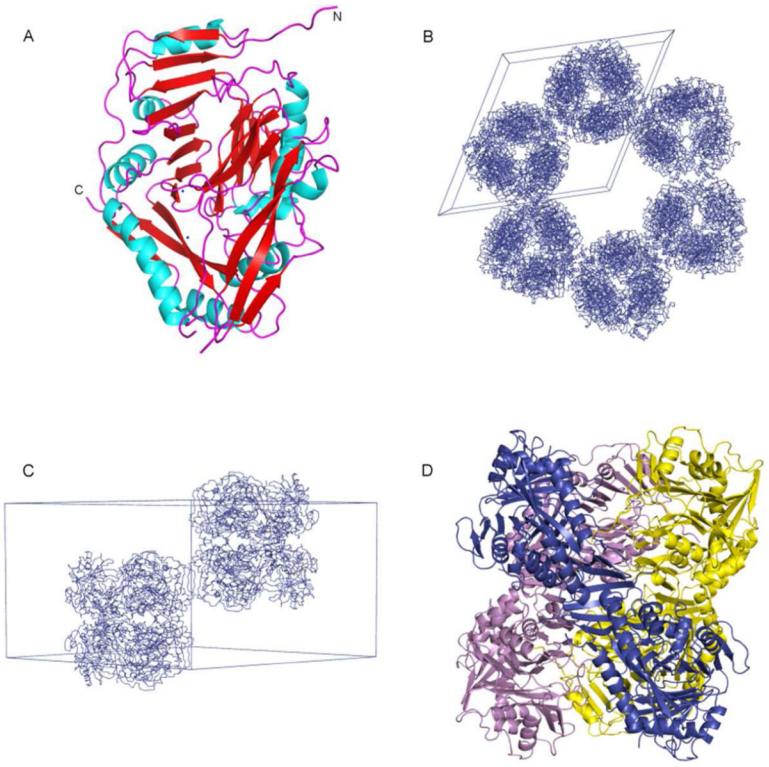

Figure 2.

Overall structure of the SmPabB monomer and illustration of the crystal packing leading to the anomalous Matthews coefficient. (A) Ribbon diagram of SmPabB colored by secondary structure. (B) Crystal packing observed for the SmPabB structure illustrating the large solvent channels present in the crystals. (C) Alternate view of the packing within the hexagonal unit cell. (D) Each unit cell contains two ‘trimers of dimers’. The dimers associate via a continuous β-sheet formed from structural elements that are believed to be disordered in the absence of substrates and/or the amidotransferase subunit PabA.

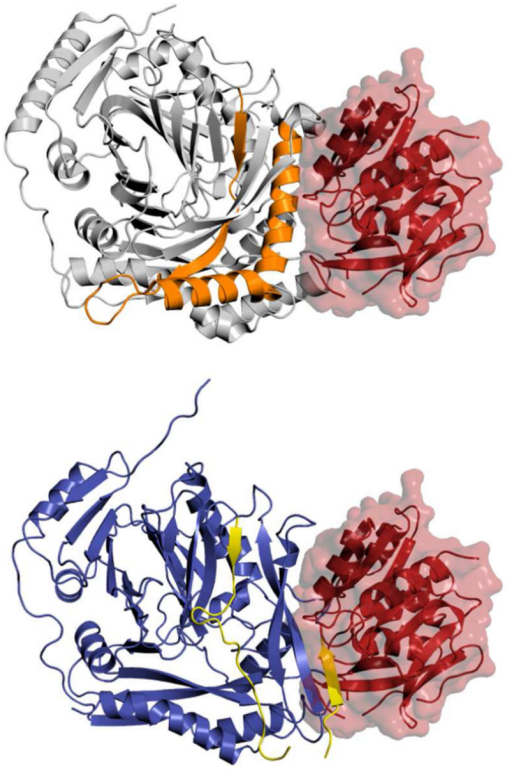

Figure 3.

SmPabB is partially disordered in the absence of substrate and PabA. The disordered region forms not only part of the active site but also key elements of the PabA-B interface. Cartoon diagrams of the TrpEG complex (1I1Q; TrpG shown in *red*, TrpE shown in *gray* except residues 319-376 shown in *orange; upper panel*) and SmPabB (*blue* except residues 267-305 shown in *yellow; lower panel*) illustrate that residues ~280-305 of SmPabB correspond to the vertical portion of the orange kinked helical segment seen in TrpE and other chorismate-utilizing enzymes. In the SmPabB structure these residues are remodeled as part of the intersubunit β-sheet structure shown in Figure 2D.

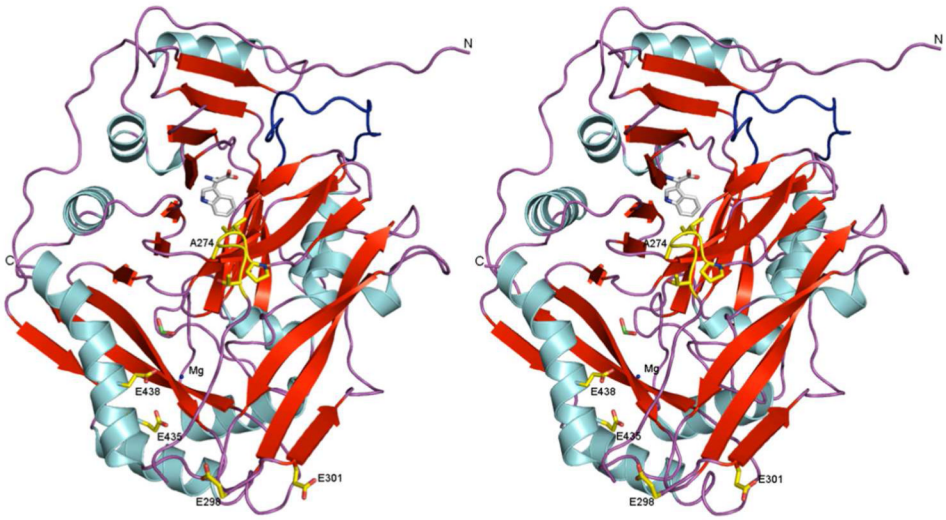

Figure 4.

Cartoon representation of the SmPabB monomer shown in stereo. A model of tryptophan illustrates the location of the putative vestigial Trp binding site. The long loop that may be associated with Trp binding and that is common to SmPabB and *E. coli* PabB but not *C. hutchinsonii* PabB is shown in dark blue. The approximate location of the catalytic Mg^{2+} ion required for catalysis is shown. Two of the four Mg^{2+} coordinating residues are observed to be in position (E435 and E438). The other two metal ligands (E298 and E301) are on the remodeled β-strand recruited for the unusual crystal packing. Also shown in yellow is the key PIAGT motif featuring A274 that occupies the position analogous to K274 in canonical PabB enzymes. The Trp, formate, and catalytic Mg^{2+} ion binding sites were modeled by superimposing SmPabB and either *E. coli* PabB (1K0E), *Serratia marcesens* TrpE (1I7Q), or *E. coli* MenF (3BZN).

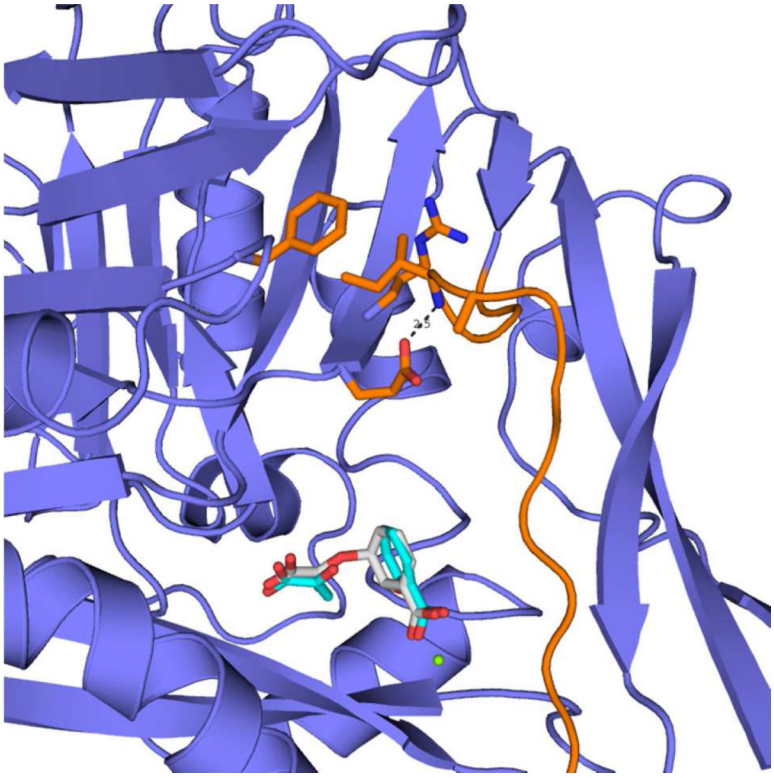

Figure 5.
Cartoon representation illustrating the interactions anchoring Ile273 and the ^{272}PI**A**GT^{277} motif in a kinked conformation away from the substrate binding site. Ile273 interacts with Glu258 via a hydrogen bond and with the side chains of Phe241 and Arg259. Isochorismate, benzoic acid, and pyruvate from EntC (3HWO) and TrpE (1I7Q) are shown to illustrate the location of the substrate binding site of SmPabB.

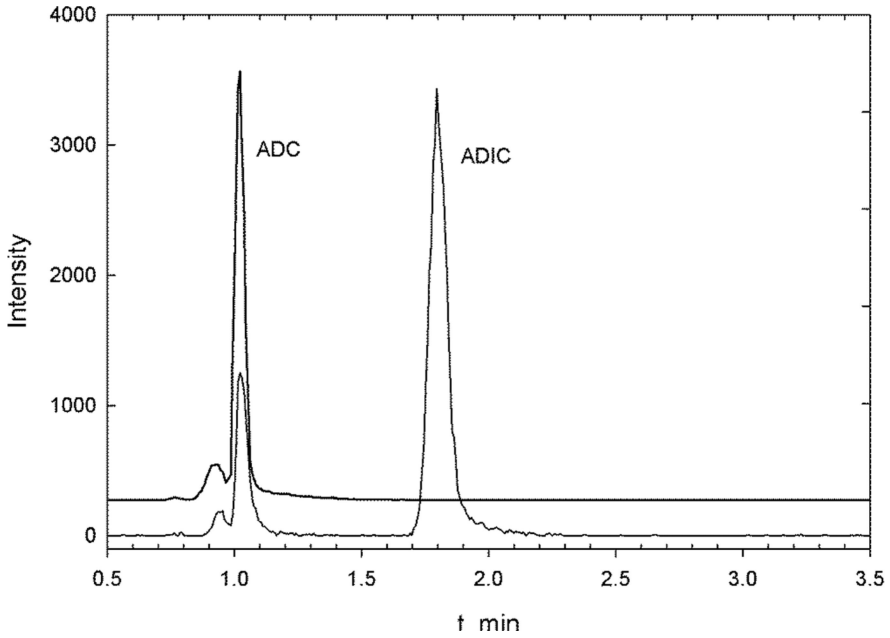

Figure 6.

Extracted ion mass chromatograms identifying ADIC as an intermediate in the SmPabB catalyzed conversion of chorismate to ADC. ADIC is present in reactions containing SmPabB but not those containing *E. coli* PabB (*offset trace*).

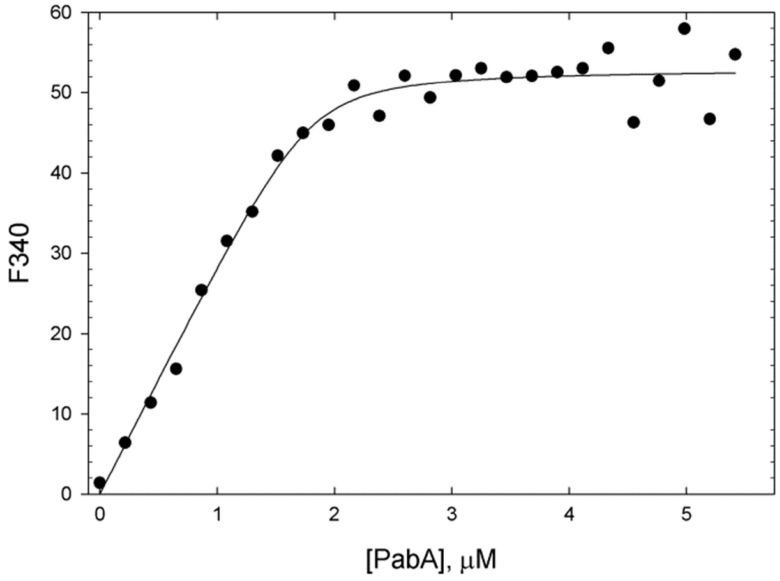

Figure 7.

Fluorescence titration experiments suggest SmPabB and *E. coli* PabA form a high affinity complex. Steady State emission spectra of SmPabB alone and in the presence of increasing amounts of PabA were recorded at 25 °C using an excitation wavelength of 285 nm. The change in fluorescence emission at 340 nm was evaluated as a function of PabA concentration by fitting the data to a quadratic function (Equation 1). Data shown above are corrected for the linear increase in fluorescence due to PabA alone. The dissociation constant determined by this method was $(3.9 \pm 3.1) \times 10^{-8}$ M.

Table 1

Data collection and Refinement Statistics

	SmPabB
PDB Code	4GRH
space group	$P6_322$
cell parameters (*a, b, c*) (Å)	161.3, 161.3, 116.1
Resolution (highest shell), (Å)	46.60-2.25 (2.33-2.25)
no. of measured intensities	1,804,918
no. of unique reflections	42,573
redundancy	42.4
completeness (%) (last shell)	100.0 (100.0)
$I/\sigma(I)$ (last shell)	20.1 (4.5)
R_{merge} % (last shell)[a]	6.2 (70.9)
refinement statistics	
resolution range (Å)	46.60-2.25
no. of reflections used	40,399
no. of protein atoms	3416
no. of waters	226
R-factor[b]	0.195
R_{free} [c]	0.240
rmsd bond lengths (Å)	0.019
rmsd bond angles (deg)	1.98
average B-factors for main chain/side chain (Å^2)	45.86/49.80

[a] $R_{merge} = \Sigma |I - (I)|/\Sigma I$, where I is the intensity of an observed reflection and (I) is the average intensity of multiple observations.

[b] $R = \Sigma||F_{obs}| - |F_{cal}||/\Sigma|F_{obs}|$.

[c] $R_{free} = \Sigma||F_{obs}| - |F_{cal}||/\Sigma|F_{obs}|$, where F_{obs} is from a test set of reflections (5 % of the total) that are not used in structural refinement.

Table 2

Results[a] of Automated Structural Alignments of SmPabB with Selected Homologs

Homolog	Cα RMSD (Å)	% identity of sequences	residues aligned
PabB (1KOG)	2.8	26	395
PabB (3H9M)	2.4	19	343
TrpE (1I7Q)	3.3	27	392
MenF (3BZN)	3.9	19	342
SS (2FN0)	3.4	23	348
EntC (3HWO)	2.8	18	300
PhzE (3R75)	2.9	21	325

[a]The software *DALI* (32) was used to perform the alignments of SmPabB with *E. coli* PabB (1K0G), *C. hutchinsonii* PabB (3H9M), *Salmonella typhimurium* TrpE (1I7Q), *E. coli* MenF (3BZN), *Yersinia enterocolitica* salicylate synthase (SS; 2FN0), *E. coli* EntC (3HWO), and *P. aeruginosa* PhzE (3R75).